Supplementary Material

Firing rate response of neocortical pyramidal neurons in the fluctuation-driven regime

Y. Zerlaut, B. Telenczuk, C. Deleuze, T. Bal, G. Ouanounou* & A. Destexhe*

January 13, 2016

Contents

1 Details about the experimental data

For each cell, its properties and the quality of the electrical access was quantified. We present here those data and look for relations between them.

Figure 1: **Details about the presented dataset (animal age, electrical access and membrane properties).** **(A)** Histogram of the access resistance. **(B)** Histogram of the "Seal Quality", the current leak between the pipette and the patch of membrane. **(C)** Histogram of the full recording time. Corresponding either to the loss of cellular access (rarely) or to the exit of the criteria formulated in Section **??** (most common case). **(D)** Histogram of the membrane time constants. **(E)** Histogram of the membrane input resistance. **(F)** Histogram of the animal post-natal day per recorded cell. **(G)** Cross correlations (Pearson corrrelation) between all monitored quantities.

Some of the relations that appear are :

- Very naturally, the membrane time constant is proportional to the input resistance (c=0.8, $p < 2.10^{-10}$)

- The recording time diminishes with the age of the animal ($p < 1.10^{-3}$)

- The membrane resistances and membrane time constants decrease with the age of the animal even if they keep a strong variability ($p < 5.10^{-3}$ and $p < 3.10^{-2}$ respectively).

- The access resistant seems independent of all parameters

- The quality of the seal does not seem to impede much the duration of the recording (despite the fact that they are both correlated with the age of the animal, there mutual correlation is low).

2   Accuracy of the single compartment approximation

The single-compartment approximation is important in this study as it is used to constrain the fluctuations of the membrane potential. We do here a cell by cell quantification of the accuracy of the approximation.

We quantify the accuracy of the approximation as follows. We take the protocols that were used to determine the membrane properties: prior to each protocol, we recorded and averaged the response to 10 current pulses of $\sim$ 500ms and of $\Delta I \sim$ 15pA amplitude, not the (noisy) continuous monitoring presented in Figure *fig-exp-charact*. We average over trials the membrane potential response and fit an exponential load to this mean response $V_{sc}^{fit}(t)$, we get a membrane time τ_m^0 and a membrane resistance R_m^0. We define the residual trace as the normalized absolute difference between the fit and the trace :

$$\mathrm{Res}(t) = \frac{\|V(t) - V_{sc}^{fit}(t)\|}{R_m^0 \Delta I} \tag{1}$$

Now we quantify the accuracy of the single-compartment approximation by taking the (normalized) integral over 7 membrane time constant of the residual trace (see bottom traces in *fig-single-comp-approx*B and *fig-single-comp-approx*C).

$$C_{sc} = \int_{t_0}^{t_0 + 7\,\tau_m^0} \frac{dt}{7\,\tau_m^0} \mathrm{Res}(t) \tag{2}$$

The two normalizations (by membrane resistance and membrane time constant) were performed to yield comparable quantities for different membrane parameters.

We present the histogram of this quantity over the cells of the dataset in Figure *fig-single-comp-approx*A.

We conclude that the approximation was satisfactory : the worst case in Figure *fig-single-comp-approx*C corresponds to a pretty good match.

../figures/single_comp.pdf

Figure 2: **Accuracy of the single compartment approximation in the neocortical neurons of our recordings.** **(A)** Histogram of the accuracy coefficient C_{sc}. **(B)** Neuron showing the best accuracy coefficient. **(C)** Neuron showing the worst accuracy coefficient.

3 Finite sampling of a Poisson process

Three main components could be identified as contributing to the measured dispersion of the firing rate dependencies. 1) cellular heterogeneity, 2) experimental changes across experiments and 3) finite sampling of the irregular firing process.

Because the cellular heterogeneity point is the biologically relevant phenomena [Mejias and Longtin, 2012] that we would like to evaluate, we try here to estimate the contribution of the finite sampling effect so that we get an higher bound for the cellular heterogeneity (higher bound because contribution of the experimental bias is unknown).

Experimentally, we estimate the firing rate on a finite amount of time T. Because the firing process is irregular, this will induce a dispersion around the mean cellular behavior.

The Poisson process has been shown to be a good model for the irregularity of the firing process **REF?**, so that this calculation will take this as an assumption. Given an ideal frequency ν evaluated over a time T, the probability to observe a frequency $\nu_{\text{obs}} = k/T$ (k is the number of observed spikes) is:

$$P_{\nu,T}(\nu_{obs} = \frac{k}{T}) = \frac{e^{-\nu T}}{T} \cdot \frac{(\nu T)^k}{k!} \tag{3}$$

Where the mean and standard deviation of observed spike number are given by: $\langle k \rangle = \nu_{\text{id}}T$ and $\sqrt{\langle (k^2 - \langle k \rangle^2) \rangle} = \sqrt{\nu_{id} T}$.

Let's say that we study the firing rate as a function of a variable x (e.g. τ_V/τ_{m}^0). We scan N points of this variable x (the x_i where $i \in [1, N]$) that we each repeat S times by varying the seed (indexed by $s \in S$). One trial result in a spike number k_i^s, therefore the whole experiment results in the set $\{k_i^s\}$. Now we assume, that the process has a well defined dependency on x (e.g. as given by 6 for τ_V/τ_{m}^0) so that the Poisson process has the frequency $\nu(x_i)$ for the trials scanning x_i. Then probability to observe the set $\{k_i^s\}$ given a finite sampling of length T (assuming independence between experiments) is:

$$P(\{k_i^s\}) = e^{-S T \sum_i \nu(x_i)} \times \Pi_i \frac{(\nu(x_i) T)^{\sum_s k_i^s}}{\Pi_s k_i^s!} \tag{4}$$

We evaluated the response heterogeneity on the coefficients of the *effective threshold* so we need to translate the set of measurements $\{k_i^s\}$ into a set of firing rate $\{\nu_i^s = k_i^s/T\}$ and then into a coefficient for the {effective threshold} (e.g. Δ_{τ_v} for τ_v/τ_{m}^0). So each possible measurement $\{k_i^s\}$ is converted into a coefficient with its probability $P(\{k_i^s\})$. We should then test for all possible measurements $\{k_i^s\}$, but in practice (because it is useless to span the whole space of possibilities), for each point, we consider values of observed spikes delimited by three standard deviations around the mean number of possible spike.

So, for each type of protocol, we take the average behavior (in terms of *phenomenological threshold*), we convert it to a firing rate thanks to the average (μ_V, σ_V, τ_V), we take the average recording conditions (number of points and seeds) and we evaluate the variations expected from those conditions (the procedure is illustrated in Figure *finite-sampling-poisson*). Because of the multiple averaging (and the fact that the expected variations are non linearly related to the *effective threshold*), the result is not exactly what would be expected from a Poisson process having this dependency but this provide a reasonable first guess.

Figure 3: **Quantifying the dispersion due to the sampling over a finite time of the irregular spiking process. Insight from the case of a Poisson process**.
(A) Let's say that the neuron has a real physical dependency of its threshold to a variable x (here a linear dependency $V_{\text{thre}}^{\text{eff}} = -50\text{mV} + (x - 1) \cdot 1$ mV). **(B)** The measurement protocol is made of varies 3 times the variable x, for 2 different seeds and for a recording time of $T = 3$s. We consider the possible spikes up to 3 standard deviations around the most probable observed spike number. **(C)** Four examples of observations (translated into the phenomenological threshold anhd with the resulting linear fit) with their respective probability (normalized to maximum). **(D)** Expected dispersion as a consequence of the finite sampling (evaluated over 50^3 observations)

4 Dependency on the first two moments of the membrane potential fluctuations

Figure 4: **Adapting a simple approximation to construct an analytical template for the firing rate response of theoretical models and neocortical neurons.** **(A)** Firing rate response of the IaF neuron in the (μ_V, σ_V) plane, the other variables were set to $\tau_V/\tau_m^0 = 45\%$ and $\mu_G/g_L = 4$ (see real units in **B**). Numerical data (points with errorbars over trials, see Methods in **??**) and fitted template. A first order polynomial of (μ_V, σ_V) was fitted for V_{thre}^{eff} (see inset plot) so that when plugged into Equation **??** it captures the firing rate response (large plain line). **(B)** We insure that the stimulation that has been designed in the Methods **??** actually brings the neuron to the desired values of $(\mu_V, \sigma_V, \tau_V, \mu_G)$, expected values are plain lines. Color code as in **A**. We performed the same numerical simulations than **A** for the subthreshold dynamics only (removing the threshold and reset mechanism) and we measure the four variables (μ_G is measured from the response to a short current step on top of the background activity, hence the noisy behavior). **(C)** Firing rate response of a single pyramidal neuron in the (μ_V, σ_V) plane. Data points and fit with the template Equation **??** (linear *phenomenological theshold* in inset). Errorbars represent standard deviation across two trials of different seed lasting 5 seconds each. **(D)** Measurements of the subthreshold variables after having clipped spikes, note that the deviations between desired and measured μ_V, σ_V and τ_V are stronger for high firing level, i.e. potentially result from the bias introduced by the clipping procedure. **(E)** Firing rate response of three other neocortical cells in the (μ_V, σ_V) plane.

We first investigate here the firing rate response as a function of the (μ_V, σ_V) variables. The stimulation designed

in the Methods *stimulation-design* allows to vary (μ_V, σ_V) independently while keeping τ_V and μ_G constant, we check on Figure *2*B (in theoretical models by removing the spiking mechanism) and Figure *2*D (by clipping spikes in the intracellular recordings) that the stimulation actually constrains μ_V and σ_V. We show on Figure *2*A the response of the IaF model. As expected given the strong non linearity of the threshold mechanism, the response is steep as a function of the fluctuations size (σ_V) at depolarized levels (high μ_V) while the firing starts at higher σ_V and is much less steep for hyperpolarized levels (low μ_V).

Introducing a linear function of μ_V and σ_V for the *phenomonological threshold* (see inset of Figure *2*A) was able to accurately describe the firing rate response of the IaF model (thick line in Figure *2*A). The correction therefore reads:

$$V_{\text{thre}}^{\text{eff}} = V_{\text{thre}}^0 + P_{\mu_V} \, \frac{\mu_V - \mu_V^0}{\delta\mu_V^0} + P_{\sigma_V} \, \frac{\sigma_V - \sigma_V^0}{\delta\sigma_V^0} \tag{5}$$

Here, to obtain comparable quantities, we have arbitrily normalized the dependency on μ_V and σ_V around a mean configuration of the *fluctuation driven* regime arbitrarily set to $\mu_V^0 = -55$mV and $\sigma_V^0 = 4$mV and the extent of their domain $\delta\mu_V^0 = 10$mV and $\delta\sigma_V^0 = 6$mV. V_{thre}^0, P_{μ_V} and P_{σ_V} are the coefficients of the linear function.

We next investigated the firing rate response of neocortical neurons as a function of the μ_V, σ_V variables (Figure *2*C and Figure *2*F). Again, an affine *phenomenological threshold* (inset in Figure *2*C) was found to be very accurate at capturing the observed firing rate response. The response of additional theoretical models and neocortical neurons in the (μ_V, σ_V) plane is visible in Figure *6*.

An individual cellular behavior corresponds to a set of coefficients V_{thre}^0, P_{μ_V} and P_{σ_V}. We show on Figure *2*F, the histogram of those coefficients across the recorded pyramidal cell population.

The first coefficient V_{thre}^0, account for a mean threshold level, it represents the mean excitability level of the neuron, we will see in the next section that it can depend on other variables. The adaptative Exponential Integrate and Fire with Regular Spiking features (AdExp-RS) shows a higher mean *phenomenological threshold* (see Figure *6*), indeed because of its finite sodium activation curve and the firing adaptation phenomena, it is less excitable that the IaF model. We see here that this mean excitability level (P_0) shows a strong heterogeneity across the recorded population, much stronger than what is predicted by only the finite sampling of the irregular spiking process (see the Methods *finite-sampling*).

The second coefficient P_{μ_V} represents the deviation from the behavior of Equation *eq-template* in the dependency to μ_V. A positive coefficient corresponds to an increasing *phenomenological threshold* with μ_V so to a reduction of the firing rate response with respect to the template. All models show a positive coefficient (see Figure *6*) so they all show an attenuated dependency with respect to the template. This attenuation is stronger for the AdExp-RS model due to 1) the adaptation mechanism (firing rate adaptation raises with the firing rate which raises with μ_V, so enhanced adaptation decreases the dependency on μ_V) and 2) the finite spike sharpness that also lowers the excitability and therefore the sensitivity to μ_V (see Figure *6*).

The third coefficient P_{σ_V} represents the deviation from the behavior of Equation **??** in the dependency to σ_V. Again, a positive coefficient corresponds to an increasing *phenomenological threshold* with σ_V so to a reduction of the firing rate response with respect to the template. Now the IaF model shows a negative coefficient (Figure *2*F), meaning the dependency on σ_V is enhanced with respect to the approximation. Here again (as for μ_V), firing adaptation and finite sharpness reduce firing rate raise with σ_V as can be seen for the AdExp-RS neuron (see Figure *6*).

5 Dependency on the speed of the subthreshold fluctuations

Figure 5: **Sensitivity to the speed of the membrane potential fluctuations.** **(A)** Firing rate response as a function of slower fluctuations speed (increasing τ_V) for 3 different models: the IaF model, the EIF model and the iLIF model. Their respective threshold have been changed to give them comparable excitabilities. **(B)** Mean, variance, input conductance and *global* autocorrelation time of the subthreshold fluctuations in absence of a spike mechanism. A shift in the mean membrane potential has been made to bring the different neurons around the same firing rate level. **(C)** Firing rate dependency on the autocorrelation time for different pyramidal neurons and for different combinations of input. Experiments are indexed as a function of the mean output rate **(D)** Measured mean, variance and global autocorrelation time after clipping spikes for the experiments shown in **C** (same color code). Within one experiment, the couple (μ_V, σ_V) should remain constant while τ_V should increase according to the dashed line. A strong shift is observed but the dependency of the deviations on the firing rate indicates that it is an effect of the clipping procedure (see the color code, from red to blue the firing rate raises as the deviations from the desired τ_V). **(F)** Effective threshold for all data of **C** with the linear fit corresponding to Equation 6. **(F)** Histogram of the experimentally measured dependency of $V_{\mathrm{thre}}^{\mathrm{eff}}$ to τ_V (i.e. P_{τ_V} coefficient) and comparison with the dependency of the models of **A**.

Because the firing rate is a temporal quantity, we expect a strong dependency of the firing to the temporal dynamics properties of the membrane potential fluctuations. It was shown in [Kuhn et al., 2004] that the firing rate can be greatly affected by the effective membrane time constant τ_{m}^{eff} for inputs leading to the same mean μ_V and variance σ_V for the subthreshold fluctuations. Nevertheless, in this study, the temporal dynamics was led by the membrane time constant and not by a mix of synaptic and membrane time constants. Because synaptic time constant are not that smaller from the effective membrane time constant (especially if we consider the low-pass filtering exerted by dendritic trees), we choose to relax this hypothesis and we investigate a domain of autocorrelation where both the synaptic and the effective membrane time constants would jointly contribute to the autocorrelation of the membrane potential fluctuations. The definition of the *global autocorrelation* time considered in this study is presented in the Methods *autocorrel-def*.

Here, the dynamic-clamp technique plays a crucial role, it allows to investigate values of the global autocorrelation that lie below the resting membrane time constant τ_{m}^0. Indeed, in the classical *current-clamp* mode, when injecting stochastic processes (see [La Camera et al., 2008] for a review), the resting membrane time constant is a lower bound for the autocorrelation time. The injection of white noise will produce an Ornstein-Uhlenbeck noise of time constant τ_{m}^0 (under the single compartment approximation) and the injection of correlated noise will produce even higher autocorrelation values. Because *in vivo*, the temporal fluctuations are faster than the resting membrane time constant (see [Destexhe et al., 2003] for a review) having an input that could reproduce this feature was crucial in our study.

We used the expressions derived in the *Methods* to design a stimulation keeping μ_V, σ_V and μ_G constant while increasing τ_V. We tested this around a mean configuration of the *fluctuation-driven* regime: $\sigma_V = 5$mV, $\mu_G = 4g_{\mathrm{L}}$ and μ_V was set to obtain a mean firing rate between 1 and 15 Hz. The characteristics of the resulting subthreshold fluctuations can be seen for single compartment model on Figure *3*B and for the data after clipping spikes in Figure *3*D.

We show on Figure *3*A this relationship for three different models: the Iaf model, the EIF model with a sharpness of $k_a = 2$mV and the inactivating leaky Integrate and Fire model (iLIF, [Platkiewicz and Brette, 2011]).

As expected in a threshold crossing situation, faster fluctuations leads to higher firing rate than slow fluctuations, we thus observe a decreasing relationship between τ_V and the firing rate. This relation is however more or less pronounced

as a function of the ability of the spiking mechanism to convert fast fluctuations into spikes. The spike sharpness creates this ability to track fast input, the reduced sharpness of the EIF model therefore result in a attenuated dependency to τ_V (see *Figure 3A*). A mechanism that penalizes the slow fluctuations also leads to an increased sensitivity to the speed of the fluctuations, the inactivation of sodium channels is such a mechanism. We show that adding an inactivation mechanism to the IaF model results in a stronger dependency to τ_V than the IaF model. This high impact of the inactivation mechanism appears because the fluctuations speed is very similar to the time constant of inactivation (~ 5ms) as would be expected *in vivo*.

For the analytical description, we found that introducing a linear dependency on τ_V in the *phenomenological* threshold was able to capture the observed behaviors. For convenience, the linear dependency is relative to the resting membrane time constant.

We introduce:

$$V_{\text{thre}}^{\text{eff}} = V_{\text{thre}}^0 + P_{\tau_V^N} \frac{\tau_V^N - \tau_V^{N0}}{\delta\tau_V^{N0}} \tag{6}$$

where P_τ accounts for the threshold dependency induced by the behavior discussed above. The higher it is, the lower the τ_V dependency (it smoothens the expected $\frac{1}{\tau_V}$ dependency). Again, this dependency is normalized with respect to a mean configuration $\tau_V^N = 0.5$ (i.e. $\tau_V = \tau_{\text{m}}^0/2$) and the extent of the τ_V^N variations: $\delta\tau_V^N = 1$.

This expression provides a quantitative way to evaluate the sensitivity to the speed of the fluctuations. Thus we investigated this sensitivity on several pyramidal neurons (*Figure 3C*). It is striking to note that the mean behavior over the cells showed a remarkable sensitivity to the *global* autocorrelation time, much stronger than the IaF model.

As suggested by the theoretical models, this high sensitivity presumably results from the combination of 1) a high ability to track fast input, close to the IaF model [Naundorf et al., 2006] [Ilin et al., 2013] and 2) a mechanism that penalizes slow fluctuating input: the inactivation of sodium channels (again revealed by the use of the *dynamic-clamp* technique that allows to produce fast membrane potential fluctuations, $\tau_V \sim 10$ms where inactivation can have a critical role).

6 Dependency on the somatic input conductance

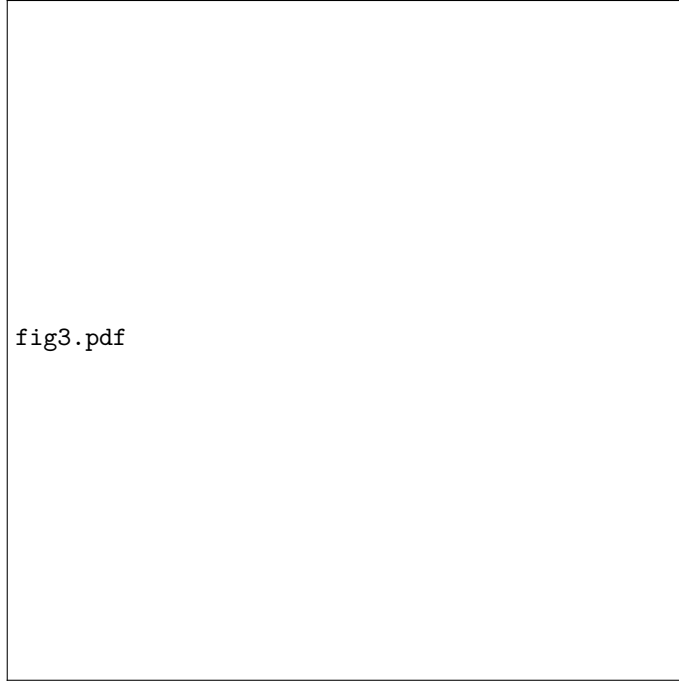Figure 6: **Increasing somatic input conductance shunts the sodium current and reduces spiking probability. (A)** Firing rate response as a response to the input varying only the total somatic conductance μ_G for the EIF model with three different spike shaprness **(B)** Insuring that the stimulation works. Mean, variance, input conductance and *global autocorrelation time* of the subthreshold fluctuations in absence of a spike mechanism. A shift in the mean membrane potential has been made to bring the different neurons around the same firing rate level (they have quite different sensitivity levels). **(C)** Firing rate dependency on the total conductance for different pyramidal neurons and for different combinations of input. Experiments are indexed as a function of the mean output rate **(D)** Measured mean, variance and global autocorrelation time after clipping spikes for the experiments shown in **C** (same color code). Within one experiment, the set of $(\mu_V, \sigma_V, \tau_V)$ should remain constant.**(F)** Effective threshold for all data of **C** with the affine fit corresponding to Equation 7. **(F)** Histogram of the experimentally measured dependency of $V_{\text{thre}}^{\text{eff}}$ to μ_G (i.e. P_{μ_G} coefficient) and comparison with the dependency of the three models of **A**.

In neocortical neurons, the spike is produced by a sodium current abruptly activated by membrane depolarisation. Under *in vivo* conditions, the somatic input conductance is greatly increased as a consequence of synaptic activity (see [Destexhe et al., 2003] for a review). Because the depolarization induced by the sodium current depends on the input conductance, it is an important question to evaluate how much the shunting of the sodium current reduces the cellular excitability as a function of an increased input conductance in the *fluctuation-driven* regime.

The minimal model exhibiting this feature is the Exponential Integrate and Fire (EIF) model. We can vary the sharpness of the spike initiation current from an infinitly sharp current ($k_a = 0$mV, IaF model), to a rather smooth spiking current ($k_a = 4$mV), see Figure *4*A. We clearly see that the spike initiation sharpness creates a decreasing dependency on the input conductance for the firing rate level.

In [Platkiewicz and Brette, 2010], in the context of their *threshold equation*, the authors proposed a way to account for this decreased excitability. We found that the mathematical expression that they proposed:

$$V_{\text{thre}}^{\text{eff}} = V_{\text{thre}}^0 + P_G \cdot \log\left(\frac{\mu_G}{g_{\text{L}}}\right) \tag{7}$$

was a good way to account for the dependency on the input conductance in our *phenomenological threshold* when introduced into the template Equation *eq-template* (note that P_G is different from k_a for the EIF model, because our *phenomenological threshold* does not correspond to the mathematically well-defined threshold of [Platkiewicz and Brette, 2010]).

We now investigate this dependency in neocortical neurons by artificial conductance increase using the *dynamic-clamp* technique (see the *Methods*). In Figure *4*C, we tested the impact of an increased input conductance at the soma on several pyramidal neurons. The accuracy of the linear description for the *phenomenological threshold* as a function of $\log(\mu_G/g_{\text{L}})$ is shown on Figure *4*E for all recorded cells. The value of all the fitted coefficients for P_{μ_G} can be seen in Figure *4*F.

It is striking to note that the mean behavior of neocortical cells can should explained by a very smooth activation curve in a single compartment model (thick black curve in Figure 4F), similar to the sodium activation curve obtained under voltage-clamp measurements (**ref?**). In addition, unlike the depdency on τ_V (Figure 3F), much of the observed variability can be explained by the finite sampling of the irregular spiking process (Figure 4F) suggesting that this feature is rather homogeneously shared within the recorded population.

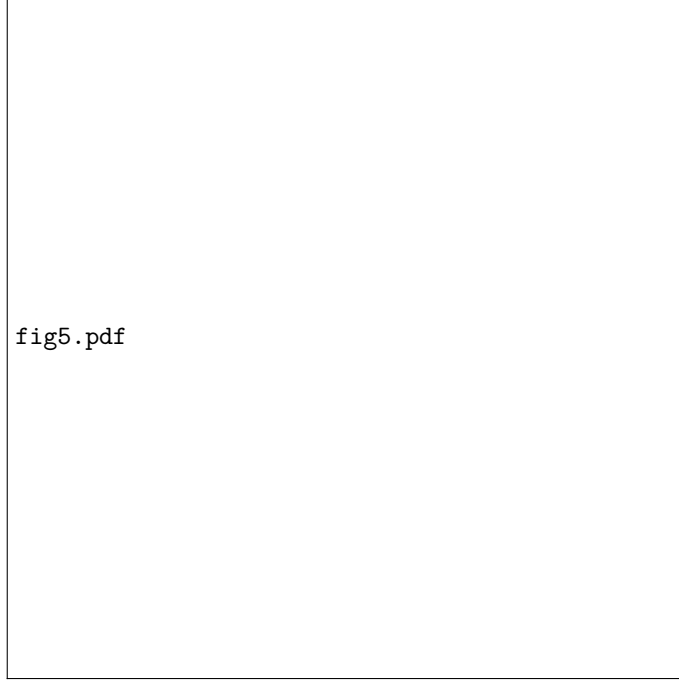# 7 Interplay of a conductance increase and faster fluctuations

Figure 7: **Firing rate as a response to an increasing input conductance and a decreasing membrane potential fluctuations speed. (A)** Firing rate response for the EIF model with three different spike sharpness ($k_a = 0$mV IaF, $k_a = 1$mV and $k_a = 2$mV). The *phenomenological threshold* can be seen in the inset. **(B)** Mean, variance, input conductance and *global* autocorrelation time of the subthreshold fluctuations in absence of a spike mechanism. A shift in the mean membrane potential has been made to bring the different neurons around the same firing rate level. In the inset, the autocorrelation function are visible as a function of the input conductance (color code) **(C)** Response of different neocortical neurons around $\sigma_V = 5$mV, $\tau_S/\tau_m^0 = 15\%$. The μ_V level was adjusted to bring the neuron in the 0-15 Hz domain. **(D)** Subthreshold variables when clipping spikes, here $\tau_V/\tau_m^0 = \tau_S/\tau_m^0 + 1/\mu_G$ **(E)** Corresponding effective thresholds. The dashed line corresponds to the mean observed dependency. **(F)** Histogram of the dependencis see in **E** with the dependencies of the theoretical models

In the two previous sections, we have investigated independently the dependency on the input conductance and the autocorrelation. A more physiological situation would correspond to a comodulation of μ_G and τ_V. Indeed, when presynaptic activity raises for fixed synaptic time constants (we discard the potential effects on μ_V and σ_V), the somatic input conductance increases and the *global autocorrelation* time decreases (Equation **??**, if $\tau_S/\tau_m^0 = \alpha = cst$ and μ_G varies, then $\tau_V/\tau_m^0 = \alpha + 1/\mu_G$). In the following for this comodulation, we will investigate this comodulation for $\tau_S/\tau_m^0 \sim 0.1$.

The two previous sections predict opposite effects as a response to this type of comodulation. Increasing conductance reduces the firing rate for non infinitely sharp activation curves and faster temporal fluctuations increase the firing rate. It is therefore important to understand what is the final output of the combination of those two effects.

For the IaF neuron, the effect is clear, the spiking mechanism does not create a dependency on μ_G then thre response to this comodulation result from the decrease of the *global autocorrelation* an leads to an increase of the firing rate (reversing Figure *3*A). On the other hand, for the EIF models, their dependency on τ_V is much weaker (EIF model on Figure *3*A), so that the competition with the decreasing dependency on μ_G leads to the almost cancellation (EIF model $k_a = 2$mV) of this increase.

We have run the same protocol on neocortical neurons, we found that the response to this comodulation is systematically increasing, still showing a high sensitivity to the speed of the fluctuations despite the potential dampening of the input conductance increase (see Figure *5*).

As this comodulation is likely to be the physiologically relevant case (though we could imagine situations where those values could vary independently, e.g. increase τ_V without μ_G by enhancing the proportion of low pass filtered distal input), we will use this to reduce the four-dimensional space to a three-dimensional space. Now variations of τ_V^N are set by varying the input conductance μ_G for a fixed τ_S/τ_m^0 i.e. we have: $\tau_V/\tau_m^0 = \tau_S/\tau_m^0 + g_L/\mu_G$. Again in the following, we will set $\tau_S/\tau_m^0 \sim 0.1$.
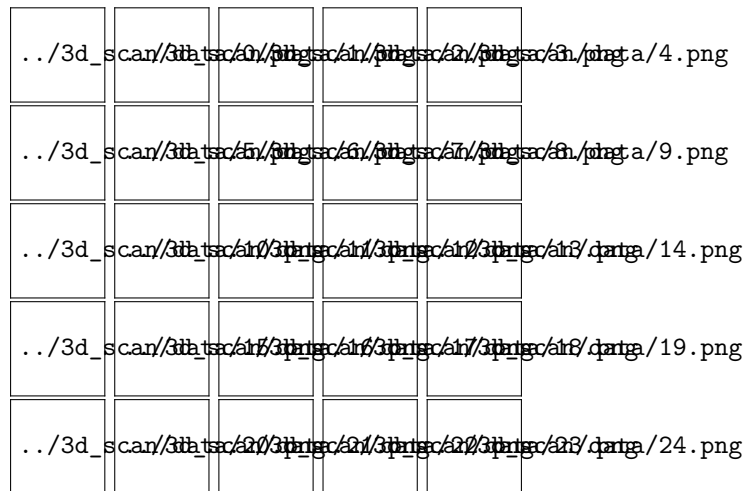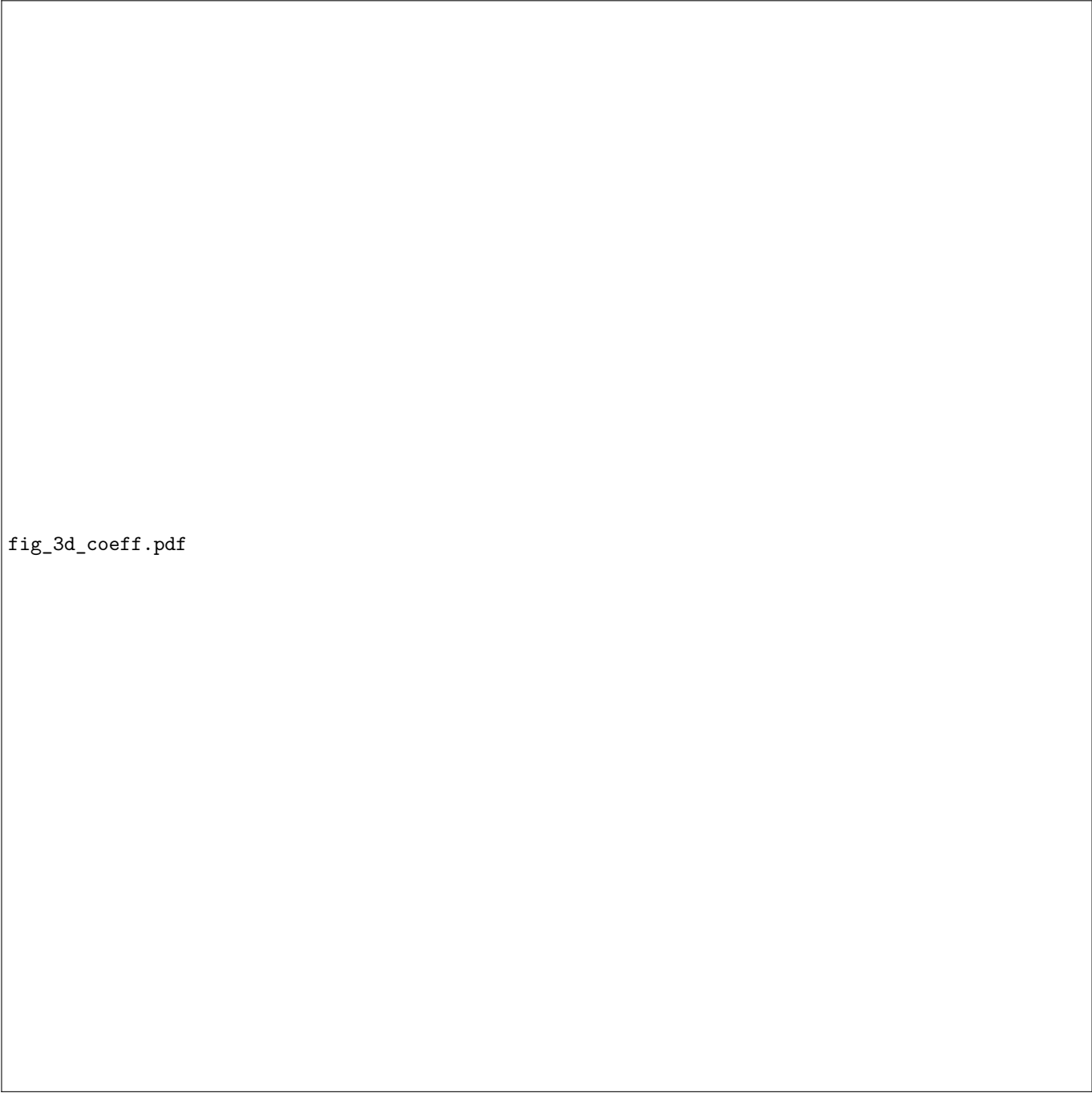
8 Full data for the 3 dimensional analysis

../3d_scan/data/0.png ../3d_scan/data/1.png ../3d_scan/data/2.png ../3d_scan/data/3.png ../3d_scan/data/4.png

../3d_scan/data/5.png ../3d_scan/data/6.png ../3d_scan/data/7.png ../3d_scan/data/8.png ../3d_scan/data/9.png

../3d_scan/data/10.png ../3d_scan/data/11.png ../3d_scan/data/12.png ../3d_scan/data/13.png ../3d_scan/data/14.png

../3d_scan/data/15.png ../3d_scan/data/16.png ../3d_scan/data/17.png ../3d_scan/data/18.png ../3d_scan/data/19.png

../3d_scan/data/20.png ../3d_scan/data/21.png ../3d_scan/data/22.png ../3d_scan/data/23.png ../3d_scan/data/24.png

Figure 8: **Full dataset (n=24) for the analysis in the $(\mu_V, \sigma_V, \tau'_V)$ space. See Section ?? .**

9   Analysis of the fitted coefficients

fig_3d_coeff.pdf

Figure 9: **Fitted coefficients for theoretical models and individual cells (generating Figure ??). (A)** PCA analysis of data. **(B)** Cross product of first component of the data with those of theoretical models of varying parameters.

10   Robustness of the firing rate characterization

The minimal number of points in the dataset of *long* recordings (presented in *fig-full-3D-data*) is n=40 points (meaning there has been 40 episodes of a given seed and a given $(\mu_V, \sigma_V, \tau_V)$.

    Here, we investigate how reliable is the characterization over this limited number of points. We do this by taking the cell having the lowest number of points

    we split the dataset into two and we check whether the sensitivity is unchanged !!

11 Nature of the observed heterogeneity, underlying structure ?

[. . .] to be written

12 Correlation between experimental conditions and functional properties

Cross correlation between the quantities calculated and presented in *exp-details*, with the functional quantities measured. . .

13 Theoretical models matching the experimental response

in the 5d params scan of the prameters, what is the model that minimize the difference with the data, what is the change of parameters that

14 References

[Destexhe et al., 2003] Destexhe, A., Rudolph, M., and Paré, D. (2003). The high-conductance state of neocortical neurons in vivo. *Nature Reviews Neuroscience*, 4(9):739–751.

[Ilin et al., 2013] Ilin, V., Malyshev, A., Wolf, F., and Volgushev, M. (2013). Fast computations in cortical ensembles require rapid initiation of action potentials. *The Journal of neuroscience : the official journal of the Society for Neuroscience*, 33(6):2281–92.

[Kuhn et al., 2004] Kuhn, A., Aertsen, A., and Rotter, S. (2004). Neuronal integration of synaptic input in the fluctuation-driven regime. *The Journal of neuroscience : the official journal of the Society for Neuroscience*, 24(10):2345–56.

[La Camera et al., 2008] La Camera, G., Giugliano, M., Senn, W., and Fusi, S. (2008). The response of cortical neurons to in vivo-like input current: theory and experiment : I. Noisy inputs with stationary statistics. *Biological cybernetics*, 99(4-5):279–301.

[Mejias and Longtin, 2012] Mejias, J. F. and Longtin, A. (2012). Optimal heterogeneity for coding in spiking neural networks. *Physical Review Letters*, 108(22):228102.

[Naundorf et al., 2006] Naundorf, B., Wolf, F., and Volgushev, M. (2006). Unique features of action potential initiation in cortical neurons. *Nature*, 440(7087):1060–3.

[Platkiewicz and Brette, 2010] Platkiewicz, J. and Brette, R. (2010). A threshold equation for action potential initiation. *PLoS computational biology*, 6(7):e1000850.

[Platkiewicz and Brette, 2011] Platkiewicz, J. and Brette, R. (2011). Impact of fast sodium channel inactivation on spike threshold dynamics and synaptic integration. *PLoS computational biology*, 7(5):e1001129.

../figures/fitting_robustness.pdf
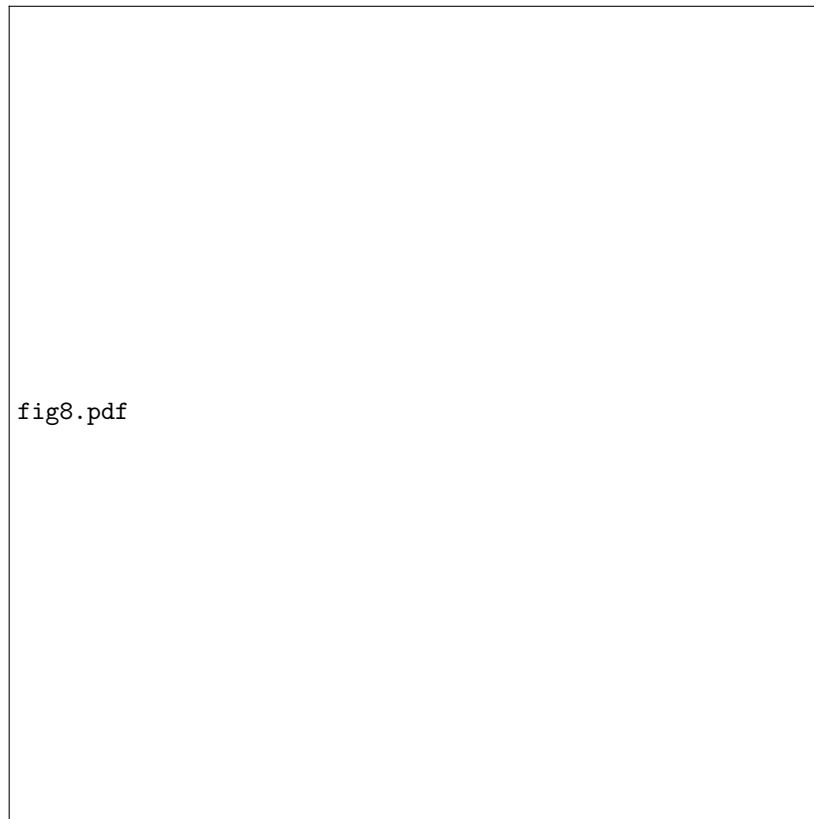
../figures/fitting_robustness2.pdf

Figure 11: **Characteristics of the measured heterogenity. (A)** PCA analysis of data. **(B)** Cross product of first component of the data with those of theoretical models of varying parameters.